

pubs.acs.org/JACS Article

Particle Swarm Predictions of a SrB₈ Monolayer with 12-Fold Metal Coordination

Xin Qu, Lihua Yang, Jian Lv,* Yu Xie, Jinghai Yang, Yukai Zhang, Yanchao Wang,* Jijun Zhao, Zhongfang Chen,* and Yanming Ma



Cite This: J. Am. Chem. Soc. 2022, 144, 11120-11128



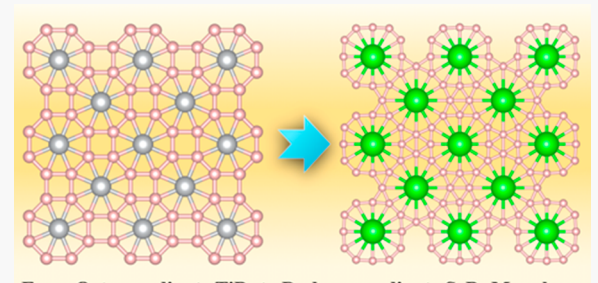
ACCESS

Metrics & More

Article Recommendations

s Supporting Information

ABSTRACT: Materials containing planar hypercoordinate motifs greatly enriched the fundamental understanding of chemical bonding. Herein, by means of first-principles calculations combined with global minimum search, we discovered the two-dimensional (2D) SrB_8 monolayer, which has the highest planar coordination number (12) reported so far in extended periodic materials. In the SrB_8 monolayer, bridged B_8 units are forming the boron monolayer consisting of B_{12} rings, and the Sr atoms are embedded at the center of these B_{12} rings, leading to the $Sr@B_{12}$ motifs. The SrB_8 monolayer has good thermodynamic, kinetic, and thermal stabilities, which is attributed to the geometry fit between the size of the Sr atom and cavity of the B_{12} rings, as well as the electron transfer from Sr atoms to electron-deficient boron network.



From Octacoordinate TiB4 to Dodecacoordinate SrB8 Monolayer

Placing the SrB_8 monolayer on the Ag(001) surface shows good commensurability of the lattices and small vertical structure undulations, suggesting the feasibility of its experimental realization by epitaxial growth. Potential applications of the SrB_8 monolayer on metal ions storage (for Li, Na, and K) are explored.

INTRODUCTION

Chemical bonding is one of the most basic concepts of chemistry. Many bonding rules were established, being foundations for the understanding of properties of molecules and solids, but at the same time several efforts have been made to challenge these well-precedented bonding rules, such as the rule-breaking planar hypercoordinate motifs. 1-3 Classically, a tetracoordinate carbon atom adopts the tetrahedral configuration with a saturated sp³ hybridization.⁴ In 1970, Hoffmann, Alder, and Wilcox proposed strategies to stabilize planar tetracoordinate carbon (ptC);⁵ in 1976, Schleyer and coworkers theoretically designed the first ptC-containing molecule;6 in 1977, Cotton and co-workers experimentally synthesized the first molecule with a ptC motif. Since then, enormous ptC-containing molecules/clusters have been theoretically designed, 1,3,8,9 and some of them have been experimentally identified, such as CAl_4^{-10} CAl_4^{2-11} and CAl₃Si^{-.12} Interestingly, the planar coordination number of carbon can be further increased to 5 and 6.13-18

Nowadays, the concept of planar hypercoordination is quite general and has been extended from carbon to other main group elements, such as boron (B), 19,20 nitrogen, 8,21 oxygen, 22,23 sulfur, 24 silicon, 25 as well as to transition metal elements. $^{26-29}$ Noteworthy, the systems with planar hypercoordination have also been expanded from molecules/clusters to periodic systems, making a significant step toward practical applications. $^{30-42}$ For example, the $\mathrm{Be_5C_2}$ monolayer with

quasi-planar pentacoordinate carbon has an unusual negative Poisson's ratio and a Dirac-like point in the band structure and thus is appealing for application in electronics and mechanics. The Cu₂Si monolayer⁴¹ containing both quasi-planar hexacoordinate Cu and Si atoms has been recently synthesized and proved to be a Dirac material promising for high-speed low-dissipation devices. 42

Boron is an element characterized by electron deficiency and versatile bonding capacity. Consequently, boron is able to adopt planar hypercoordinate configurations with various elements including itself. ^{43,44} Both small-sized planar B clusters and two-dimensional (2D) B sheets have been experimentally realized, ^{44–48} in which the planar hexacoordinate B moiety is the basic building block. Strikingly, a team led by Wang and Boldyrev identified planar hepta- and octacoordinate B in wheel-type geometries of $B_8^{\,2-}$ and $B_9^{\,-}$ clusters. ^{19,20} Inspired by this discovery, they proposed geometric and electronic factors for rational design of borometallic molecular wheels and realized a series of transition-metal-centered borometallic molecular wheels, such as $FeB_8^{\,-26}$ $FeB_9^{\,-26}$ $CoB_8^{\,-27}$ $RuB_9^{\,-27}$

Received: December 28, 2021 Published: June 16, 2022





 $RhB_{97}^{28}~IrB_{97}^{28}~NbB_{10}^{-,29}$ and $TaB_{10}^{-,29}$ where the limit of planar coordination number was push to 10 in NbB_{10}^{-} and $TaB_{10}^{-,50}$

Thus far, the highest planar coordination number reported for isolated systems is 13, which is recently found in the LaC₁₃⁺ cluster,⁵¹ while the number in extended periodic materials is lower, being eight in 2D FeB₆ ³² and TiB₄ ³⁴ monolayers. The continuing considerable interest in finding planar hypercoordinate structures leads to a natural question: what is the highest planar coordination number that we can achieve?⁵⁰ In this work, we push the limit of planar coordination number in periodic materials to 12 by designing a 2D strontium boride (SrB₈) monolayer by means of first-principles calculations. The proposed SrB₈ monolayer can be constructed by placing Sr atoms and D_{2h} B₈ units on square lattices, where two types of Sr@B₁₂ wheels are formed with planar dodecacoordinate Sr atom located at the center of 12-membered B rings. The SrB₈ monolayer exhibits good thermodynamic, kinetic, and thermal stabilities, which are attributed to the electron transfer from Sr to the B framework. The metallicity and abundant adsorption sites nature of SrB₈ monolayer enable its potential applications as anode material for rechargeable metal ion batteries.

COMPUTATIONAL METHODS

All the calculations were performed in the framework of density functional theory. For isolated molecules, structure optimizations, frequency analyses, and electronic structure calculations were performed at the B3LYP/6-31G(d, p) level of theory using the Gaussian 09 package. 52 For 2D periodic systems, the structure optimizations and molecular dynamics simulations were carried out using the plane wave basis set with projected augmented wave and PBE exchange-correlation functional as implemented in the Vienna ab initio simulation package (VASP).55 The 3s²3p⁶4s², 4s²4p⁶5s², 5s²5p⁶6s², and 2s²2p¹ electrons for Ca, Sr, Ba, and B atoms were treated as valence electrons, respectively. The electronic properties were calculated using the hybrid HSE06 functional.⁵⁶ The cutoff energy of 600 eV for wave function expansion and the Monkhorst-Pack k-point sampling were chosen to ensure that the total energy converges ~1 meV per atom. 2D monolayers were placed in the xy plane with the z direction perpendicular to the layer plane, and a vacuum space of 20 Å in the z direction was adopted to avoid interactions between the adjacent layers. Phonon calculations were carried out using the frozen phonon approach as implemented in the PHONOPY package.⁵⁷ Ab initio molecular dynamics (AIMD) simulations were performed at different temperatures up to 3000 K to evaluate the thermal stability of the 2D monolayer. The initial configuration was taken from the optimized structure at zero temperature with a 3 × 3 supercell. Each AIMD simulation in the NVT ensemble lasted for 40 ps with a time step of 2.0 fs, and the temperature was controlled by using the Nosé-Hoover

The swarm-intelligence-based CALYPSO method and code ^{59–63} were employed for searching low-energy 2D Sr–B monolayers. Its validity has been manifested by successful identification of the ground-state structures for a large number of systems. ^{64–67} In the CALYPSO calculations, the simulation cells containing up to 4 formula units were considered. The population size was set to 50, and more than 1000 structures were sampled on the potential energy surface for each stoichiometry in the 2D planar space.

■ RESULTS AND DISCUSSION

Design of 2D Monolayer Materials with Planar Dodecacoordinate Configuration. The design of a 2D monolayer with planar dodecacoordinate configuration was initially inspired by our recent discovery of the TiB_4 monolayer with P4/mmm symmetry, 34 in which each Ti atom binds to

eight B atoms with equal distance in a perfect plane, featuring planar octacoordinate configurations (Figure 1a). The basic

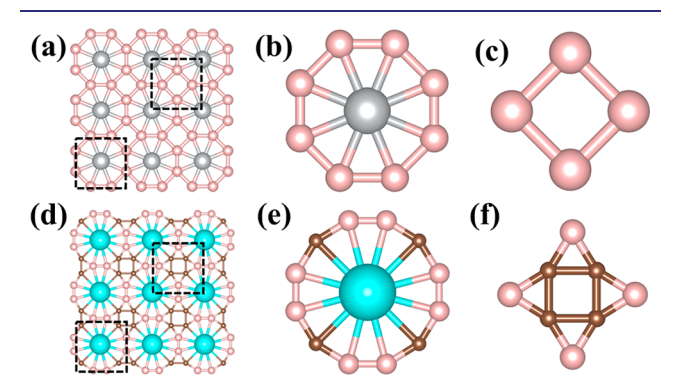


Figure 1. Sketch map from the octacoordinate TiB_4 structure to a designed dodecacoordinate structure. Structures of (a) a TiB_4 monolayer with building blocks of (b) a D_{8h} $\mathrm{Ti@B}_8$ wheel and (c) a B_4 square. Structures of (d) a MB_8 monolayer with building blocks of (e) a D_{12h} $\mathrm{M@B}_{12}$ wheel and (f) D_{4h} four-pointed-star-like B_8 unit. The pink, brown, gray and cyan balls represent B, inserted B, Ti, and undetermined metal (M) atoms, respectively. The black dashed line denotes a unit cell.

building blocks in the TiB₄ monolayer are the D_{8h} Ti@B₈ wheel and the B₄ square (Figure 1b and Figure 1c); both are arranged on the corner of 2D square lattices. The D_{8h} Ti@B₈ wheels connect to each other by sharing B–B edges, while the B₄ squares join each other through B–B bonds. Leaving out the electronic factor, a simple and straightforward way to construct a 2D monolayer with higher number of planar coordination is to use larger metal-centered B wheels, e.g., a D_{12h} M@B₁₂, and place them on a square lattice similar to that in the TiB₄ monolayer. This allows us to construct a P4/mmm MB₈ structure with perfect planar dodecacoordinate configuration (Figure 1d), which contains building blocks of a D_{12h} M@B₁₂ wheel and a four-pointed-star-like B₈ unit (Figure 1e and Figure 1f).

Finding a promising building block candidate and then assembling the candidate in a 2D plane are two important steps of the bottom-up strategy, which is one of the three main strategies for designing rule-breaking 2D materials (the other two strategies are isoelectronic substitution and direct global minimum search).³² Now we have preliminarily assembled building blocks in a 2D plane; however, whether the four-pointed-star-like B₈ unit building block is a good candidate or not has not been evaluated.

Inspiringly, the D_{2h} B₈ unit was found in a D_{2h} B₈H₄ antiaromatic molecule, ⁶⁸ and D_{2h} B₈ units also appeared in other hypercoordinate structures such as FeB₆ ³² and MnB₆. ³³ Thus, the B₈ unit might play key roles in mapping out the planar hypercoordinate materials and is worth more detailed studies.

To check the suitability of B_8 units as building blocks in the designed MB_8 structure, we investigated the geometric and electronic structures of the four-pointed-star-like B_8 unit with D_{4h} (designed in this work) and D_{2h} (literature reported) symmetries. The same as previous studies, ⁶⁸ the four corner B atoms in D_{4h} and D_{2h} star-like B_8 units were saturated by hydrogen atoms, resulting in D_{4h} and D_{2h} B_8H_4 molecules (Figure 2). We optimized their structures with different charge and spin states at the B3LYP/6-311+G* level of theory. Our computations showed that the D_{2h} B_8H_4 molecule is ~1.61

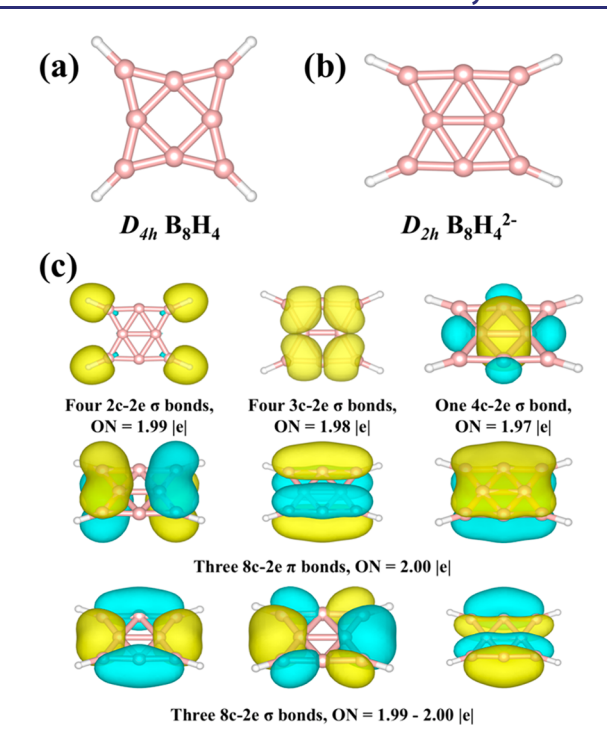


Figure 2. Structures of (a) a D_{4h} B₈H₄ molecule constructed by terminated a D_{4h} star-like B₈ unit with four H atoms, and (b) a D_{2h} B₈H₄²⁻ molecule obtained by locally optimizing the D_{4h} B₈H₄ at -2 charge and singlet state. (c) Chemical bonding analyses of the D_{2h} B₈H₄²⁻ through AdNDP. The pink and white balls represent B and H atoms, respectively.

kcal/mol lower in energy than the D_{4h} B₈H₄ molecule, and the D_{2h} configuration (Figure 2b) is a local minimum only with -2 charge at the singlet state. Within the singlet D_{2h} B₈H₄²⁻ molecule, all the atoms reside in a plane with the eight B atoms forming six triangles arranged in a rectangular shape. The B–B bond lengths are in range of 1.60–1.74 Å.

To understand the stability of the D_{2h} $B_8H_4^{2-}$ singlet ground state, we analyzed the chemical bonding using the adaptive natural density partitioning (AdNDP). The AdNDP analysis (Figure 2c) revealed four localized two-center—two-electron (2c—2e) B—H σ bonds. The remaining σ electron densities are partitioned into three sets of delocalized σ bonds: four 3c—2e σ bonds, one 4c—2e σ bond, and three 8c—2e σ bonds. All the π electron density could be divided into three delocalized 8c—2e bonds, which renders π aromaticity according to the (4N + 2) Hückel rule with N=1 and is responsible for the stability of the planar geometry of the molecule. Scrutinizing the canonical molecular orbitals (Figure S1) of D_{2h} $B_8H_4^{2-}$ further supports the above AdNDP analysis.

The discovery of the dynamically stable D_{2h} $B_8H_4^{2-}$ with planar geometry motivated us to further design planar hypercoordinate 2D monolayers by placing the new B_8 units and metal atoms in the aforementioned patterns. Two types of MB_8 structures can be constructed depending on how the four B_8 units are orientated around a metal atom. As depicted in Figure 3, the first structure (Figure 3a) possesses a square lattice and P4/mmm symmetry, in which adjacent B_8 units are perpendicular to each other, and the second structure (Figure 3b) has a rectangle lattice with Cmmm symmetry, where the B_8 units are arranged in parallel. In the P4/mmm structure, there are two types of $M@B_{12}$ wheels, while in the Cmmm structure there is only one type of $M@B_{12}$ wheel.

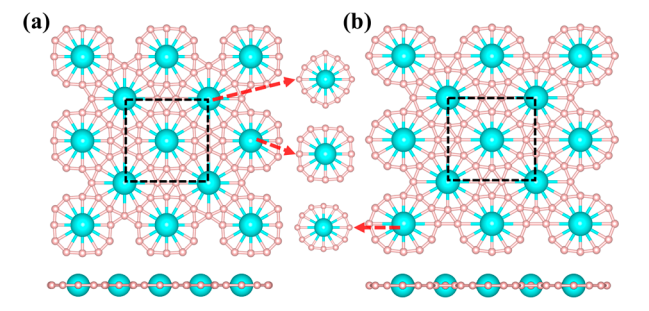


Figure 3. Top and side views of the two designed MB_8 monolayers with planar dodecacoordinate metal atoms: (a) P4/mmm MB_8 and (b) Cmmm MB_8 . The different types of $M@B_{12}$ wheels are illustrated between the two structures. The pink and cyan balls represent B and undetermined metal (M) atoms, respectively. The black dashed line denotes a unit cell.

To stabilize these two planar structures, it is important to choose a suitable metal atom. Here, +2 valence heavy alkali earth atoms, i.e., Ca, Sr, and Ba, are of good choice since they have atomic radii larger than Fe³² and Ti, ³⁴ which are favorable for achieving a coordination number higher than eight, since the radius of the metal atom in the dodecacoordinate configuration is expected to be larger than that in the octacoordinated configuration. Meanwhile, these metal atoms might offer several electrons to the B₈ units. Therefore, we performed geometry optimizations and phonon calculations for CaB₈, SrB₈, and BaB₈ monolayers with both P4/mmm and Cmmm space groups. As shown in Figure S2, CaB₈ and BaB₈ monolayers are not dynamically stable as indicated by significant imaginary frequencies in the phonon dispersion curves. Encouragingly, both P4/mmm and Cmmm structures of SrB₈ monolayer are local minima without appreciable imaginary frequencies.

Global minimum search is another well used strategy to design 2D rule-breaking hypercoordinate materials. Inspired by our above finding that metal atom and boron atom with the stoichiometry of 1:8 is able to form planar dodecacoordinate configurations, we performed the global minimum search of the Sr–B system in 2D planar space using the CALYPSO method. The stoichiometries of $Sr_{1-x}B_x$ (x = 1/3, 2/5, 1/2, 3/5, 2/3, 5/7, 3/4, 4/5, 6/7, 8/9, and 10/11) were systematically searched. By full structural relaxations, the global minimum structures for each stoichiometry were obtained (Figure S3), and the thermodynamic stability of different $Sr_{1-x}B_x$ was evaluated by the formation energy (E_f) defined as

$$E_{\rm f} = E_{\rm Sr_{1-x}B_x} - (1-x)E_{\rm Sr} - xE_{\rm B}$$

where $E_{\rm Sr_{1-x}B_x}$ and $E_{\rm Sr}$ are the total energies of ${\rm Sr_{1-x}B_x}$ and bulk Sr, respectively; $E_{\rm B}$ represents the total energy of either the α -B monolayer or bulk rhombohedral B. (Note that the B monolayer has already been synthesized through deposition of atomized vapor, $^{46-48}$ and the α -B monolayer usually serves as a common choice as reference when evaluating the stabilities of B-containing 2D materials. $^{70-72}$) On the basis of the $E_{\rm f}$ of different stoichiometries, the convex hulls for Sr–B system with different B references were constructed (Figure S4). It is found that regardless of the choice of the B references, the relative stabilities for Sr–B systems show a similar trend: generally, the stability of 2D Sr–B systems increases as the B concentration increases; SrB₅, SrB₆, and SrB₈ species have rather similar stabilities; the SrB₈ monolayer is among the most

stable stoichiometries, which has a lower formation than that of α -B monolayer and is stable against decomposition into other Sr–B systems.

Most importantly, our structure searches successfully reproduced the P4/mmm and Cmmm SrB₈ monolayers, and the former is found to be the global minimum. Other low-lying SrB₈ monolayers from the structure search are shown in Figure S5, along with their symmetries and energies relative to the global minimum. Note that some low-lying structures (structures III and IV in Figure S5) have B rings (B₁₀ rings) smaller than those in the designed P4/mmm and Cmmm structures (B₁₂ rings). Such structures cannot restore planar geometries after out-of-plane distortions along with geometric optimizations. This further demonstrates the geometry fit between the size of the Sr atom and the cavity of the B₁₂ rings in the P4/mmm and Cmmm SrB₈ structures. Free energy calculations for low-lying structures in Figure S5 were performed under the harmonic approximation using PHO-NOPY code,⁵⁷ and the results (Figure S6) indicate that the P4/mmm structure has the lowest free energy at finite temperatures. We also performed preliminarily global minimum search for Ca-B and Ba-B systems with the stoichiometry of 1:8. It was easy to predict new structures with lower energy than P4/mmm and Cmmm structures of CaB₈ and BaB₈ monolayers, manifesting that Ca and Ba are not suitable for constructing stable dodecacoordinate configurations, as we concluded by our dynamic stability evaluations.

As the P4/mmm SrB₈ configuration is the lowest energy structure in 2D plane space in our CALYPSO prediction, we will mainly focus on the P4/mmm SrB₈ monolayer in the following sections.

Stability and Synthesizability of the P4/mmm SrB₈ Monolayer. The optimized P4/mmm SrB₈ monolayer consists of two Sr atoms and 16 B atoms in a unit cell with lattice parameters of a = b = 8.43 Å. The two Sr atoms occupy the 1b (0, 0, 0.5) and 1d (0.5, 0.5, 0.5) sites, respectively; the 16 B atoms occupy the 4m (0, 0.39, 0.5), 4o (0.5, 0.83, 0.5), and 8p (0.31, 0.18, 0.5) sites, respectively. Each Sr atom is coordinated to 12 B atoms, exhibiting planar dodecacoordinate configurations. The Sr–B and B–B distances are in range of 2.80–3.29 Å and 1.57–1.83 Å, which are close to those in the crystal SrB₆ (3.08 and 1.76 Å for Sr–B and B–B bond lengths, respectively).

To examine the thermal stability, we performed AIMD simulations for the P4/mmm SrB₈ monolayer. Six independent AIMD simulations (at 300, 500, 1000, 1500, 2000, and 2500 K) were carried out using a 3×3 supercell (containing 162) atoms). The snapshots of the SrB₈ monolayer taken at the end of 20 ps simulations are given in Figure S7. The topological structure of the P4/mmm SrB₈ remains with only moderate in/ out-of-plane deformations up to 2000 K, suggesting that P4/ mmm SrB_o is separated from other minimum structures by high energy barriers. The distorted structures can restore the planar structure after geometry optimization. As the temperature increases, the distortions become more and more pronounced, and the network of the P4/mmm SrB₈ is destroyed at an extremely high temperature of 2500 K. The well-preserved structure of the P4/mmm SrB₈ at such a high temperature of up to 2000 K demonstrates its remarkable stability against thermal perturbation.

We also considered several wrinkled structures by displacing Sr and/or B atoms of the P4/mmm SrB₈ monolayer along the out-of-plane direction by a small distance. The distorted

structures spontaneously transform into a pure plane after geometry optimization, implying the robustness of the planar P4/mmm structure.

The thermodynamic stability of the P4/mmm SrB₈ monolayer can be evaluated in term of cohesive energy (E_c). The E_c can be accessed by

$$E_{\rm c} = (E_{\rm Sr} + 8E_{\rm B} - E_{{\rm Sr}B_{\rm g}})/9$$

where $E_{\rm SrB_8}$ is the total energy of the P4/mmm SrB₈ monolayer, $E_{\rm Sr}$ and $E_{\rm B}$ are the energies of isolated Sr and B atoms, respectively. According to this definition, a more positive $E_{\rm c}$ value indicates higher thermodynamic stability. The calculated $E_{\rm c}$ of the SrB₈ monolayer is 5.46 eV, which is comparable to or higher than those of Fe–B (5.79–4.87 eV), 32,74 Be–C (4.82–4.58 eV), 38,75 Al–C (5.1–3.97 eV), 76,77 and Cu₂Si (3.46 eV) monolayers at the same theoretical level. The relatively high cohesive energy of the P4/mmm SrB₈ monolayer suggests its strongly bonded network.

The lack of precursor in bulk Sr–B compound (SrB₆) rules out the top-down exfoliation approach for the synthesis of the P4/mmm SrB₈ monolayer. Therefore, we explored the feasibility of the bottom-up method by which the SrB₈ monolayer is epitaxially grown on suitable substrates through deposition as already established for the synthesis of silicene and borophene. We found that it is easy to build coperiodic lattices of the SrB₈ monolayer on Au(001), Ag(001), and Al(001) metal substrates: the lattice mismatches (δ) between 1 × 1 SrB₈ and the 2 × 2 Au(001), Ag(001), and Al(001) slab substrates are only 1.40%, 1.66%, and 4.17%, respectively. Herein the lattice mismatch is calculated as

$$\delta = \frac{2|L_{\text{mol}} - L_{\text{sub}}|}{L_{\text{mol}} + L_{\text{sub}}} \times 100\%$$

where $L_{\rm mol}$ and $L_{\rm sub}$ represent the lattice parameters of the SrB₈ monolayer and the metal (001) face substrates, respectively. The good lattice parameter match between the SrB₈ monlayer and the metal substrates can efficiently lower the strain, which facilitates the synthesis of SrB₈. As shown in Figure S8 and Table S1, in the optimized structures of SrB₈ on metal (001) substrates, the original geometry of the SrB₈ monolayer is well maintained with only slight buckling. Among the three examined SrB₈-metal (001) systems, SrB₈-Ag(001) has the smallest undulation (0.42 Å) for the SrB₈ plane and the largest interlayer distance (2.22 Å), indicating the relative weak interfacial interaction between SrB₈ and Ag(001).

Moreover, the exfoliation energy could estimate whether the ${\rm SrB_8}$ monolayer is easy to be peeled off from substrates, and it might be calculated as the difference between the total energy of ${\rm SrB_8-metal}$ (001)-face system and the sum of the energies of metal slab substrate and isolated ${\rm SrB_8}$ monolayer. The exfoliation energy of ${\rm SrB_8}$ on ${\rm Ag}(001)$ (41.32 meV/Ų) is comparable with those of the most recently synthesized 2D boron sheets on Ag surface (about 30–50 eV/Ų). Thus, once grown epitaxially on the ${\rm Ag}(001)$ surface, the asfabricated ${\rm SrB_8}$ monolayer may be easily peeled off from the substrate in postgrowth separation process.

However, our MD simulations (Figure S9) indicate that the framework of the SrB_8 would be destroyed upon O_2 adsorption. Therefore, additional efforts, such as ligand passivation, might be needed to increase the stability of the SrB_8 upon exposure to the air.

Electronic Properties of the P4/mmm SrB₈ Monolayer. To gain deeper insight into the mechanism for the stability of the P4/mmm SrB₈ monolayer, we investigated its electronic structures. Figure 4 presents the electron localization

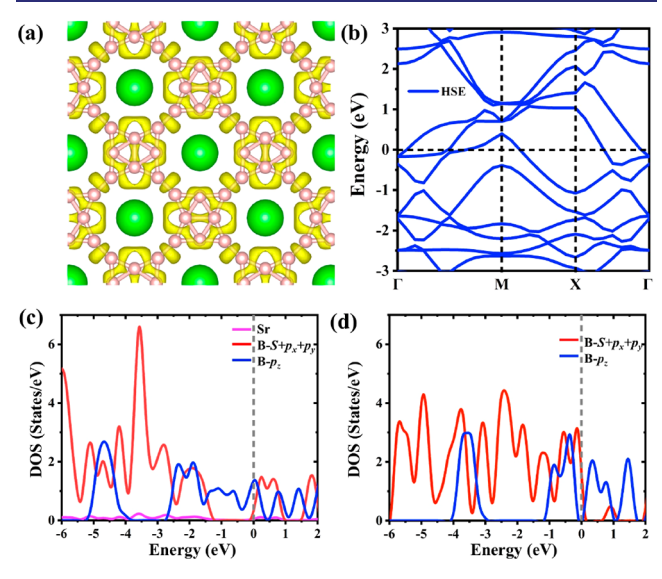


Figure 4. (a) Isosurface of ELF with a value of 0.75, (b) electronic band structure, and (c) the projected density of states (PDOS) of the P4/mmm SrB₈ monolayer. (d) PDOS of the bare B network in the P4/mmm SrB₈ monolayer. The pink and green balls in (a) represent B and Sr atoms, respectively.

function (ELF),⁷⁹ band structure, and projected density of states (PDOS) calculated using the hybrid HSE06 functional (the data using the PBE functional gives consistent results as shown in Figure S10). The isosurface of ELF with a value of 0.75 (Figure 4a) demonstrates that electrons mainly accumulate at the B framework. The D_{2h} B₈ units are bonded by delocalized multicenter bonds, which is reminiscent of that in small planar B clusters. The B₈ units connect each other through classic 2c-2e B-B σ bonds. The Bader charge 80 calculation indicates each Sr donates ~1.66 e to the B framework (the Bader charge is usually less than the formal oxidation number). Given that the Sr atom generally shows an oxidation state of +2 and there is an equal number of Sr atoms and the B₈ units in the SrB₈, it is reasonable to conclude that each B₈ unit accepts two electrons from the Sr atoms. Therefore, the bonding situation of the B₈ units should be same as that in the aromatic $B_8H_4^{\ 2-}$ molecule, which is responsible for the planarity of the SrB₈ monolayer.

The calculated electronic band structure (Figure 4b) demonstrates the metallic nature of the SrB_8 monolayer as evidenced by the bands across the Fermi level at Γ -M, M-X, and Γ -X directions. The PDOS analysis shows that Sr atoms have negligible contribution to the valence bands and mainly account for the high-energy conduction bands above 2 eV. This is consistent with the results of ELF and Bader charge analysis, which indicate that the Sr atom donates about 2 valence electrons to the B framework. The Fermi level is located at the gap between the bonding and antibonding states of in-plane orbitals (B-s, B-p_x and B-p_y) and cuts the out-of-plane states of B-p_z orbital, which is consistent with a previous analysis on the stability of 2D B sheets. ⁸¹ If we remove the Sr atoms from the SrB_8 monolayer, the PDOS of the resulting bare B framework (Figure 4d) shows substantial unoccupied

in-plane states with a peak located at the Fermi level, which will destabilize the 2D B framework. Therefore, in addition to the geometric fit between the size of Sr atom and cavity of the B rings, electron transfer from Sr to the B framework is crucial for the stabilization of the SrB₈ monolayer.

We further looked into the chemical bonding of the SrB_8 monolayer through the solid state adaptive natural density partitioning (SSAdNDP) method. ⁸² In our calculations (Figure 5), one unit cell of SrB_8 (2 Sr atoms and 16 B

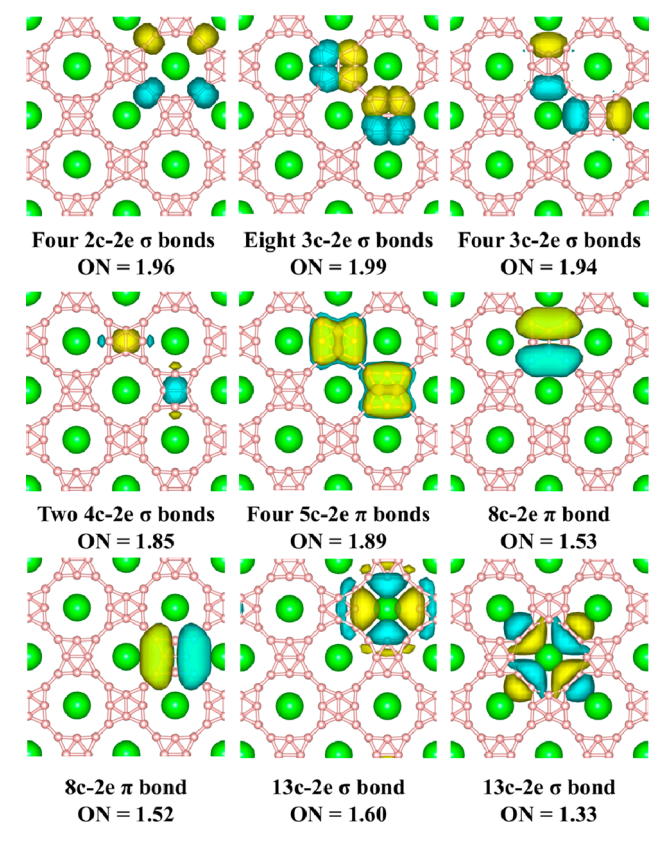


Figure 5. SSAdNDP chemical bonding patterns of the ${\rm SrB_8}$ monolayer.

atoms) monolayer contains four $2c-2e\ \sigma$ bonds, $12\ 3c-2e\ \sigma$ bonds, two $4c-2e\ \sigma$ bonds, four $5c-2e\ \pi$ bonds, two $8c-2e\ \pi$ bonds, and two $13c-2e\ \sigma$ bonds, accounting for 52 electrons per unit cell. The classic 2c-2e bonds are responsible for the strong connections between the B_8 units, while the abundance of multicenter bonds contributes significantly to the high stability of the whole network. The SSAdNDP results are consistent with those of the ELF and Bader charge.

The unique planar geometric structure and intrinsic metallicity of the *P4/mmm* SrB₈ monolayer also motivated us to perform preliminary calculations to explore its potential as an anode material for lithium (Li), sodium (Na), and potassium (K) ion batteries. As shown in the section "Potential of the *P4/mmm* SrB₈ Monolayer as an Anode Material for Alkali Metal Ion Batteries" in the Supporting Information, the relatively low diffusion energy barrier, high specific capacity and suitable open circuit voltage of Li, Na, and K suggest that the predicted SrB₈ monolayer may be a promising anode material for metal ion batteries.

CONCLUSION

In summary, by detailed analysis of the B₈ building blocks and comprehensive first-principles calculations combined with global minimum optimizations, we identified a rather stable atomically thin planar P4/mmm SrB₈ monolayer with the record high coordination number of 12 for the central transition metal atom. The SrB₈ monolayer contains two types of $Sr@B_{12}$ wheels with a planar dodecacoordinate Sratom located at the center of 12-membered B rings and has good thermodynamic, dynamic, and thermal stabilities. The emergence of this planar structure is attributed to a geometric fit between the size of the Sr atom and the cavity of the B rings, as well as electron transfer from Sr atoms to the B framework. The SrB₈ monolayer on Ag(001) substrate nearly retains the same structure as in vacuum. The small lattice mismatch and moderate exfoliation energy of SrB₈ monolayer on the Ag(001) substrate suggest that it is highly feasible to experimentally realize this unique 2D material through the chemical vapor deposition or molecular beam epitaxy method. This work provides new guidelines for the rational design of novel 2D materials and pushes the coordination number in the materials with planar hypercoordination motifs to a new record of 12. If synthesized, the P4/mmm SrB₈ monolayer may serve as promising anode materials for alkali metal ion batteries. We hope that this work will greatly inspire further explorations of materials with novel chemical bonding and motivate more investigations on designing 2D materials with hypercoordinate motifs.

ASSOCIATED CONTENT

Supporting Information

The Supporting Information is available free of charge at https://pubs.acs.org/doi/10.1021/jacs.1c13654.

> Calculated canonical molecular orbitals of the D_{2h} B₈H₄²⁻ molecule; phonon dispersion curves of CaB₈, SrB₈, and BaB₈ monolayers; structures (in molecular dynamics simulations, on substrates, and with adsorption atoms); electronic properties of the SrB₈ monolayer; results of the P4/mmm SrB₈ monolayer for ions storage (PDF)

AUTHOR INFORMATION

Corresponding Authors

Jian Lv - International Center for Computational Method and Software, State Key Laboratory of Superhard Materials, Key Laboratory of Physics and Technology for Advanced Batteries, Ministry of Education, College of Physics, Jilin University, Changchun 130012, China; o orcid.org/0000-0002-6201-9888; Email: lyjian@calypso.cn

Yanchao Wang - International Center for Computational Method and Software, State Key Laboratory of Superhard Materials, Key Laboratory of Physics and Technology for Advanced Batteries, Ministry of Education, College of Physics, Iilin University, Changchun 130012, China; oorcid.org/ 0000-0003-4518-925X; Email: wyc@calypso.cn

Zhongfang Chen - Department of Chemistry, University of Puerto Rico, Rio Piedras Campus, San Juan, Puerto Rico 00931, United States; orcid.org/0000-0002-1445-9184; Email: zhongfang.chen1@upr.edu

Authors

Xin Qu - International Center for Computational Method and Software, State Key Laboratory of Superhard Materials, Key Laboratory of Physics and Technology for Advanced Batteries, Ministry of Education, College of Physics, Jilin University, Changchun 130012, China; Key Laboratory of Functional Materials Physics and Chemistry of the Ministry of Education, Key Laboratory of Preparation and Application of Environmental Friendly Materials, College of Physics, Jilin Normal University, Changchun 130103, China

Lihua Yang - International Center for Computational Method and Software, State Key Laboratory of Superhard Materials, Key Laboratory of Physics and Technology for Advanced Batteries, Ministry of Education, College of Physics, Jilin University, Changchun 130012, China; Key Laboratory of Functional Materials Physics and Chemistry of the Ministry of Education, Key Laboratory of Preparation and Application of Environmental Friendly Materials, College of Physics, Jilin Normal University, Changchun 130103, China

Yu Xie - International Center for Computational Method and Software, State Key Laboratory of Superhard Materials, Key Laboratory of Physics and Technology for Advanced Batteries, Ministry of Education, College of Physics, Jilin University, Changchun 130012, China; orcid.org/0000-0002-7782-5428

Jinghai Yang - Key Laboratory of Functional Materials Physics and Chemistry of the Ministry of Education, Key Laboratory of Preparation and Application of Environmental Friendly Materials, College of Physics, Jilin Normal University, Changchun 130103, China; orcid.org/0000-0001-8409-6035

Yukai Zhang — Key Laboratory of Functional Materials Physics and Chemistry of the Ministry of Education, Key Laboratory of Preparation and Application of Environmental Friendly Materials, College of Physics, Jilin Normal University, Changchun 130103, China

Jijun Zhao - Key Laboratory of Materials Modification by Laser, Ion and Electron Beams, Dalian University of Technology, Dalian 116024, China; orcid.org/0000-0002-3263-7159

Yanming Ma – International Center for Computational Method and Software, State Key Laboratory of Superhard Materials, Key Laboratory of Physics and Technology for Advanced Batteries, Ministry of Education, College of Physics, Jilin University, Changchun 130012, China

Complete contact information is available at: https://pubs.acs.org/10.1021/jacs.1c13654

Author Contributions

 $^{\perp}$ X.Q. and L.Y. contributed equally.

The authors declare no competing financial interest.

ACKNOWLEDGMENTS

X.Q. is thankful to Min Zhang and Changyan Zhu for valuable discussions. This work was supported in China by National Natural Science Foundation of China (Grants 91961204, 12034009, 11974134, 11904129, and 12174142), the Thirteenth Five-Year Program for Science and Technology of Education Department of Jilin Province (Grant JJKH20200408KJ), the Program for the Development of Science and Technology of Jilin Province (Grant YDZJ202101ZYTS065), the Open Project of State Key Laboratory of Superhard Materials (Jilin University, Grant 201908), and in USA by the NSF Center for the Advancement of Wearable Technologies (Grant 1849243). Part of the calculations were performed at the high-performance computing center of Jilin University and Tianhe2-JK at the Beijing Computational Science Research Center. This paper is dedicated to the 70th anniversary of the physics of Jilin University.

REFERENCES

- (1) Yang, L.-M.; Ganz, E.; Chen, Z.; Wang, Z.-X.; Schleyer, P. V. R. Four Decades of the Chemistry of Planar Hypercoordinate Compounds. *Angew. Chemie Int. Ed.* **2015**, *54* (33), 9468–9501.
- (2) Vassilev-Galindo, V.; Pan, S.; Donald, K. J.; Merino, G. Planar Pentacoordinate Carbons. *Nat. Rev. Chem.* **2018**, 2 (2), 0114.
- (3) Merino, G.; Méndez-Rojas, M. A.; Vela, A.; Heine, T. Recent Advances in Planar Tetracoordinate Carbon Chemistry. *J. Comput. Chem.* **2007**, 28 (1), 362–372.
- (4) Monkhorst, H. J. Activation Energy for Interconversion of Enantiomers Containing an Asymmetric Carbon Atom without Breaking Bonds. *Chem. Commun.* **1968**, 1111–1112.
- (5) Hoffmann, R.; Alder, R. W.; Wilcox, C. F. Planar Tetracoordinate Carbon. J. Am. Chem. Soc. 1970, 92 (16), 4992–4993
- (6) Collins, J. B.; Dill, J. D.; Jemmis, E. D.; Apeloig, Y.; Schleyer, P. v. R.; Seeger, R.; Pople, J. A. Stabilization of Planar Tetracoordinate Carbon. J. Am. Chem. Soc. 1976, 98 (18), 5419–5427.
- (7) Cotton, F. A.; Millar, M. The Probable Existence of a Triple Bond between Two Vanadium Atoms. *J. Am. Chem. Soc.* **1977**, 99 (24), 7886–7891.
- (8) von Ragué Schleyer, P.; Boldyrev, A. I. A New, General Strategy for Achieving Planar Tetracoordinate Geometries for Carbon and Other Second Row Periodic Elements. *J. Chem. Soc., Chem. Commun.* 1991, 1536–1538.
- (9) Siebert, W.; Gunale, A. Compounds Containing a Planar-Tetracoordinate Carbon Atom as Analogues of Planar Methane. *Chem. Soc. Rev.* **1999**, 28 (6), 367–371.
- (10) Li, X.; Wang, L. S.; Boldyrev, A. I.; Simons, J. Tetracoordinated Planar Carbon in the Al₄C⁻ Anion. A Combined Photoelectron Spectroscopy and Ab Initio Study. *J. Am. Chem. Soc.* **1999**, *121* (25), 6033–6038.
- (11) Li, X.; Zhang, H.-F. F.; Wang, L.-S. S.; Geske, G. D.; Boldyrev, A. I. Pentaatomic Tetracoordinate Planar Carbon, $[CAl_4]^2$: A New Structural Unit and Its Salt Complexes. *Angew. Chemie Int. Ed.* **2000**, 39 (20), 3630–3632.
- (12) Wang, L. S.; Boldyrev, A. I.; Li, X.; Simons, J. Experimental Observation of Pentaatomic Tetracoordinate Planar Carbon-Containing Molecules. *J. Am. Chem. Soc.* **2000**, *122* (32), 7681–7687.
- (13) Exner, K.; Schleyer, P. v. R. Planar Hexacoordinate Carbon: A Viable Possibility. *Science* **2000**, 290 (5498), 1937–1940.
- (14) Wang, Z.-X.; Schleyer, P. v. R. Construction Principles of "Hyparenes": Families of Molecules with Planar Pentacoordinate Carbons. *Science* **2001**, 292 (5526), 2465–2469.
- (15) Ito, K.; Chen, Z.; Corminboeuf, C.; Wannere, C. S.; Zhang, X. H.; Li, Q. S.; Schleyer, P. v. R. Myriad Planar Hexacoordinate Carbon Molecules Inviting Synthesis. *J. Am. Chem. Soc.* **2007**, *129* (6), 1510–1511.
- (16) Pei, Y.; An, W.; Ito, K.; Schleyer, P. V. R.; Zeng, X. C. Planar Pentacoordinate Carbon in $\mathrm{CAl_5}^{(+)}$: A Global Minimum. *J. Am. Chem. Soc.* **2008**, *130* (31), 10394–10400.
- (17) Merino, G.; Méndez-Rojas, M. A.; Beltrán, H. I.; Corminboeuf, C.; Heine, T.; Vela, A. Theoretical Analysis of the Smallest Carbon Cluster Containing a Planar Tetracoordinate Carbon. *J. Am. Chem. Soc.* **2004**, *126* (49), 16160–16169.
- (18) Merino, G.; Méndez-Rojas, M. A.; Vela, A. $(C_5M_{2-n})^{n-}$ (M = Li, Na, K, and n = 0, 1, 2). A New Family of Molecules Containing Planar Tetracoordinate Carbons. *J. Am. Chem. Soc.* **2003**, 125 (20), 6026–6027.

- (19) Zhai, H. J.; Alexandrova, A. N.; Birch, K. A.; Boldyrev, A. I.; Wang, L. S. Hepta- and Octacoordinate Boron in Molecular Wheels of Eight- and Nine-Atom Boron Clusters: Observation and Confirmation. *Angew. Chemie Int. Ed.* **2003**, *42* (48), 6004–6008.
- (20) Averkiev, B. B.; Boldyrev, A. I.; Li, X.; Wang, L.-S. Planar Nitrogen-Doped Aluminum Clusters Al_xN^- (X = 3-5). *J. Chem. Phys.* **2006**, 125 (12), 124305.
- (21) Nayak, S. K.; Rao, B. K.; Jena, P.; Li, X.; Wang, L. S. Observation of a Spin-Protected High-Energy Isomer of Al_4N^- Cluster. *Chem. Phys. Lett.* **1999**, 301 (3–4), 379–384.
- (22) Li, S.-D.; Ren, G.-M.; Miao, C.-Q.; Jin, Z.-H. M_4H_4X : Hydrometals (M=Cu, Ni) Containing Tetracoordinate Planar Nonmetals (X=B, C, N, O). *Angew. Chem., Int. Ed.* **2004**, 43 (11), 1371–1373.
- (23) Zhang, X. M.; Lv, J.; Ji, F.; Wu, H. S.; Jiao, H.; Schleyer, P. V. R. A Perfectly Square-Planar Tetracoordinated Oxygen in a Tetracopper Cluster-Based Coordination Polymer. *J. Am. Chem. Soc.* **2011**, *133* (13), 4788–4790.
- (24) Müller, A.; Henkel, G. [Ni₅S(SBu^t)₅]⁻ and [Ni₃S-(SBu^t)₃(CN)₃]²⁻, Novel Complexes with Sulfur-Capped, Thiolate-Bridged Polygonal Metal Frames. *Chem. Commun.* **1996**, 1005–1006.
- (25) Li, S. D.; Miao, C. Q.; Guo, J. C.; Ren, G. M. Planar Tetra-, Penta-, Hexa-, Hepta-, and Octacoordinate Silicons: A Universal Structural Pattern. J. Am. Chem. Soc. 2004, 126 (49), 16227–16231.
- (26) Romanescu, C.; Galeev, T. R.; Sergeeva, A. P.; Li, W. L.; Wang, L. S.; Boldyrev, A. I. Experimental and Computational Evidence of Octa- and Nona-Coordinated Planar Iron-Doped Boron Clusters: Fe©B₈ and Fe©B₉. J. Organomet. Chem. **2012**, 721–722, 148–154.
- (27) Romanescu, C.; Galeev, T. R.; Li, W. L.; Boldyrev, A. I.; Wang, L. S. Aromatic Metal-Centered Monocyclic Boron Rings: CoB₈⁻ and RuB₉⁻. *Angew. Chemie Int. Ed.* **2011**, *50* (40), 9334–9337.
- (28) Li, W.-L.; Romanescu, C.; Galeev, T. R.; Piazza, Z. A.; Boldyrev, A. I.; Wang, L.-S. Transition-Metal-Centered Nine-Membered Boron Rings: $M@B_9^-$ and $M@B_9^-$ (M = Rh, Ir). *J. Am. Chem. Soc.* **2012**, *134* (1), 165–168.
- (29) Galeev, T. R.; Romanescu, C.; Li, W. L.; Wang, L. S.; Boldyrev, A. I. Observation of the Highest Coordination Number in Planar Species: Decacoordinated Ta©B₁₀⁻ and Nb©B₁₀⁻ Anions. *Angew. Chemie Int. Ed.* **2012**, *51* (9), 2101–2105.
- (30) Wang, Y.; Li, Y.; Chen, Z. Planar Hypercoordinate Motifs in Two-Dimensional Materials. Acc. Chem. Res. 2020, 53 (4), 887–895.
- (31) Pancharatna, P. D.; Mendez-Rojas, M. A.; Merino, G.; Vela, A.; Hoffmann, R. Planar Tetracoordinate Cabon in Extended Systems. *J. A.m. Chem. Soc.* **2004**, *126* (46), 15309.
- (32) Zhang, H.; Li, Y.; Hou, J.; Tu, K.; Chen, Z. FeB₆ Monolayers: The Graphene-like Material with Hypercoordinate Transition Metal. *J. Am. Chem. Soc.* **2016**, 138 (17), 5644–5651.
- (33) Zhang, X.; Zhang, Z.; Zhao, X.; Wu, D.; Zhou, Z. MnB_x Monolayers with Quasi-Planar Hypercoordinate Mn Atoms and Unique Magnetic and Mechanical Properties. *FlatChem.* **2017**, *4*, 42–47
- (34) Qu, X.; Yang, J.; Wang, Y.; Lv, J.; Chen, Z.; Ma, Y. A Two-Dimensional TiB₄ Monolayer Exhibits Planar Octacoordinate Ti. *Nanoscale* **2017**, *9*, 17983–17990.
- (35) Wu, X.; Pei, Y.; Zeng, X. C. B₂C Graphene, Nanotubes, and Nanoribbons. *Nano Lett.* **2009**, *9* (4), 1577–1582.
- (36) Luo, X.; Yang, J.; Liu, H.; Wu, X.; Wang, Y.; Ma, Y.; Wei, S. H.; Gong, X.; Xiang, H. Predicting Two-Dimensional Boron-Carbon Compounds by the Global Optimization Method. *J. Am. Chem. Soc.* **2011**, *133* (40), 16285–16290.
- (37) Zhang, Z.; Liu, X.; Yakobson, B. I.; Guo, W. Two-Dimensional Tetragonal TiC Monolayer Sheet and Nanoribbons. *J. Am. Chem. Soc.* **2012**, 134 (47), 19326–19329.
- (38) Wang, Y.; Li, F.; Li, Y.; Chen, Z. Semi-Metallic Be₅C₂ Monolayer Global Minimum with Quasi-Planar Pentacoordinate Carbons and Negative Poisson's Ratio. *Nat. Commun.* **2016**, *7*, 11488. (39) Li, Y.; Li, F.; Zhou, Z.; Chen, Z. SiC₂ Silagraphene and Its One-Dimensional Derivatives: Where Planar Tetracoordinate Silicon Happens. *J. Am. Chem. Soc.* **2011**, *133* (4), 900–908.

- (40) Zhou, L. J.; Zhang, Y. F.; Wu, L. M. SiC₂ Siligraphene and Nanotubes: Novel Donor Materials in Excitonic Solar Cells. *Nano Lett.* **2013**, *13* (11), 5431–5436.
- (41) Yang, L. M.; Bačić, V.; Popov, I. A.; Boldyrev, A. I.; Heine, T.; Frauenheim, T.; Ganz, E. Two-Dimensional Cu₂Si Monolayer with Planar Hexacoordinate Copper and Silicon Bonding. *J. Am. Chem. Soc.* **2015**, *137* (7), 2757–2762.
- (42) Feng, B.; Fu, B.; Kasamatsu, S.; Ito, S.; Cheng, P.; Liu, C.-C.; Feng, Y.; Wu, S.; Mahatha, S. K.; Sheverdyaeva, P.; et al. Experimental Realization of Two-Dimensional Dirac Nodal Line Fermions in Monolayer Cu₂Si. *Nat. Commun.* **2017**, *8* (1), 1007.
- (43) Romanescu, C.; Galeev, T. R.; Li, W. L.; Boldyrev, A. I.; Wang, L. S. Transition-Metal-Centered Monocyclic Boron Wheel Clusters ($M@B_n$): A New Class of Aromatic Borometallic Compounds. *Acc. Chem. Res.* **2013**, 46 (2), 350–358.
- (44) Sergeeva, A. P.; Popov, I. A.; Piazza, Z. A.; Li, W. L.; Romanescu, C.; Wang, L. S.; Boldyrev, A. I. Understanding Boron through Size-Selected Clusters: Structure, Chemical Bonding, and Fluxionality. *Acc. Chem. Res.* **2014**, *47* (4), 1349–1358.
- (45) Sun, X.; Liu, X.; Yin, J.; Yu, J.; Li, Y.; Hang, Y.; Zhou, X.; Yu, M.; Li, J.; Tai, G.; et al. Two-Dimensional Boron Crystals: Structural Stability, Tunable Properties, Fabrications and Applications. *Adv. Funct. Mater.* **2017**, 27 (19), 1603300.
- (46) Mannix, A. J.; Zhou, X.-F. X. F.; Kiraly, B.; Wood, J. D.; Alducin, D.; Myers, B. D.; Liu, X.; Fisher, B. L.; Santiago, U.; Guest, J. R.; et al. Synthesis of Borophenes: Anisotropic, Two-Dimensional Boron Polymorphs. *Science*. **2015**, *350* (6267), 1513–1516.
- (47) Feng, B.; Zhang, J.; Zhong, Q.; Li, W.; Li, S.; Li, H.; Cheng, P.; Meng, S.; Chen, L.; Wu, K. Experimental Realization of Two-Dimensional Boron Sheets. *Nat. Chem.* **2016**, *8* (6), 563–568.
- (48) Tai, G.; Hu, T.; Zhou, Y.; Wang, X.; Kong, J.; Zeng, T.; You, Y.; Wang, Q. Synthesis of Atomically Thin Boron Films on Copper Foils. *Angew. Chemie Int. Ed.* **2015**, *54* (51), 15473–15477.
- (49) Romanescu, C.; Galeev, T. R.; Li, W. L.; Boldyrev, A. I.; Wang, L. S. Geometric and Electronic Factors in the Rational Design of Transition-Metal-Centered Boron Molecular Wheels. *J. Chem. Phys.* **2013**, *138* (13), 134315.
- (50) Heine, T.; Merino, G. What Is the Maximum Coordination Number in a Planar Structure? *Angew. Chemie Int. Ed.* **2012**, *51* (18), 4275–4276.
- (51) Lu, X. Q.; Lu, H. G.; Li, S. D. Metal-Centered Monocyclic Carbon Wheel Clusters with Record Coordination Numbers in Planar Species. *RSC Adv.* **2021**, *11* (44), 27193–27198.
- (52) Frisch, M. J.; Trucks, G. W.; Schlegel, H. B.; Scuseria, G. E.; Robb, M. A.; Cheeseman, J. R.; Scalmani, G.; Barone, V.; Mennucci, B.; Petersson, G. A.; Nakatsuji, H.; Caricato, M.; Li, X.; Hratchian, H. P.; Izmaylov, A. F.; Bloino, J.; Zheng, G.; Sonnenberg, J. L.; Hada, M.; Ehara, M.; Toyota, K.; Fukuda, R.; Hasegawa, J.; Ishida, M.; Nakajima, T.; Honda, Y.; Kitao, O.; Nakai, H.; Vreven, T.; Montgomery, J. A.; Peralta, J. E.; Ogliaro, F.; Bearpark, M.; Heyd, J. J.; Brothers, E.; Kudin, K. N.; Staroverov, V. N.; Kobayashi, R.; Normand, J.; Raghavachari, K.; Rendell, A.; Burant, J. C.; Iyengar, S. S.; Tomasi, J.; Cossi, M.; Rega, N.; Millam, J. M.; Klene, M.; Knox, J. E.; Cross, J. B.; Bakken, V.; Adamo, C.; Jaramillo, J.; Gomperts, R.; Stratmann, R. E.; Yazyev, O.; Austin, A. J.; Cammi, R.; Pomelli, C.; Ochterski, J. W.; Martin, R. L.; Morokuma, K.; Zakrzewski, V. G.; Voth, G. A.; Salvador, P.; Dannenberg, J. J.; Dapprich, S.; Daniels, A. D.; Farkas, O.; Foresman, J. B.; Ortiz, J. V.; Cioslowski, J.; Fox, D. J. Gaussian 09; Gaussian, Inc.: Wallingford, CT, 2009.
- (53) Blöchl, P. E. Projector Augmented-Wave Method. *Phys. Rev. B* **1994**, *50* (24), 17953–17979.
- (54) Perdew, J. P.; Burke, K.; Ernzerhof, M. Generalized Gradient Approximation Made Simple. *Phys. Rev. Lett.* **1996**, 77 (18), 3865–3868.
- (55) Kresse, G.; Furthmüller, J. Efficient Iterative Schemes for Ab Initio Total-Energy Calculations Using a Plane-Wave Basis Set. *Phys. Rev. B* **1996**, *54* (16), 11169–11186.

- (56) Heyd, J.; Scuseria, G. E.; Ernzerhof, M. Hybrid Functionals Based on a Screened Coulomb Potential. *J. Chem. Phys.* **2003**, *118* (18), 8207–8215.
- (57) Togo, A.; Tanaka, I. First Principles Phonon Calculations in Materials Science. Scr. Mater. 2015, 108, 1–5.
- (58) Martyna, G. J.; Klein, M. L.; Tuckerman, M. Nosé-Hoover Chains: The Canonical Ensemble via Continuous Dynamics. *J. Chem. Phys.* **1992**, *97* (4), 2635–2643.
- (59) Wang, Y.; Lv, J.; Zhu, L.; Ma, Y. Crystal Structure Prediction via Particle-Swarm Optimization. *Phys. Rev. B Condens. Matter Mater. Phys.* **2010**, 82 (9), 094116.
- (60) Wang, Y.; Miao, M.; Lv, J.; Zhu, L.; Yin, K.; Liu, H.; Ma, Y. An Effective Structure Prediction Method for Layered Materials Based on 2D Particle Swarm Optimization Algorithm. *J. Chem. Phys.* **2012**, *137* (22), 224108.
- (61) Lv, J.; Wang, Y.; Zhu, L.; Ma, Y. Particle-Swarm Structure Prediction on Clusters. J. Chem. Phys. 2012, 137 (8), 084104.
- (62) Wang, Y.; Lv, J.; Zhu, L.; Ma, Y. CALYPSO: A Method for Crystal Structure Prediction. *Comput. Phys. Commun.* **2012**, *183* (10), 2063–2070.
- (63) Gao, B.; Gao, P.; Lu, S.; Lv, J.; Wang, Y.; Ma, Y. Interface Structure Prediction via CALYPSO Method. *Sci. Bull.* **2019**, *64* (5), 301–309.
- (64) Wang, Y.; Lv, J.; Zhu, L.; Lu, S.; Yin, K.; Li, Q.; Wang, H.; Zhang, L.; Ma, Y. Materials Discovery via CALYPSO Methodology. *J. Phys.: Condens. Matter* **2015**, *27* (20), 203203.
- (65) Wang, H.; Wang, Y.; Lv, J.; Li, Q.; Zhang, L.; Ma, Y. CALYPSO Structure Prediction Method and Its Wide Application. *Comput. Mater. Sci.* **2016**, *112*, 406–415.
- (66) Peng, F.; Sun, Y.; Pickard, C. J.; Needs, R. J.; Wu, Q.; Ma, Y. Hydrogen Clathrate Structures in Rare Earth Hydrides at High Pressures: Possible Route to Room-Temperature Superconductivity. *Phys. Rev. Lett.* **2017**, *119* (10), 107001.
- (67) Li, Y. Y.; Hao, J.; Liu, H.; Li, Y. Y.; Ma, Y. The Metallization and Superconductivity of Dense Hydrogen Sulfide. *J. Chem. Phys.* **2014**, *140* (17), 174712.
- (68) Li, D. Z.; Lu, H. G.; Li, S. D. Planar π -Aromatic C_{3h} $B_6H_3^+$ and π -Antiaromatic C_{2h} B_8H_2 : Boron Hydride Analogues of D_{3h} $C_3H_3^+$ and D_{2h} C_4H_4 . *J. Mol. Model.* **2012**, *18* (7), 3161–3167.
- (69) Zubarev, D. Y.; Boldyrev, A. I. Developing Paradigms of Chemical Bonding: Adaptive Natural Density Partitioning. *Phys. Chem. Phys.* **2008**, *10* (34), 5207.
- (70) Song, B.; Zhou, Y.; Yang, H.-M.; Liao, J.-H.; Yang, L.-M.; Yang, X.-B.; Ganz, E. Two-Dimensional Anti-Van't Hoff/Le Bel Array AlB₆ with High Stability, Unique Motif, Triple Dirac Cones, and Superconductivity. *J. Am. Chem. Soc.* **2019**, *141* (8), 3630–3640.
- (71) Yu, J.; Khazaei, M.; Umezawa, N.; Wang, J. Evolutionary Structure Prediction of Two-Dimensional IrB_{14} : A Promising Gas Sensor. *J. Mater. Chem. C* **2018**, *6*, 5803–5811.
- (72) Liao, J. H.; Zhao, Y. C.; Zhao, Y. J.; Xu, H.; Yang, X. B. Phonon-Mediated Superconductivity in Mg Intercalated Bilayer Borophenes. *Phys. Chem. Chem. Phys.* **2017**, *19* (43), 29237–29243.
- (73) Ott, H. R.; Chernikov, M.; Felder, E.; Degiorgi, L.; Moshopoulou, E. G.; Sarrao, J. L.; Fisk, Z. Structure and Low Temperature Properties of SrB₆. Zeitschrift für Phys. B Condens. Matter **1997**, 102 (3), 337–345.
- (74) Zhang, H.; Li, Y.; Hou, J.; Du, A.; Chen, Z. Dirac State in the FeB₂ Monolayer with Graphene-Like Boron Sheet. *Nano Lett.* **2016**, 16 (10), 6124–6129.
- (75) Li, Y.; Liao, Y.; Chen, Z. Be₂C Monolayer with Quasi-Planar Hexacoordinate Carbons: A Global Minimum Structure. *Angew. Chemie Int. Ed.* **2014**, 53 (28), 7248–7252.
- (76) Dai, J.; Wu, X.; Yang, J.; Zeng, X. C. Al_xC Monolayer Sheets: Two-Dimensional Networks with Planar Tetracoordinate Carbon and Potential Applications as Donor Materials in Solar Cell. *J. Phys. Chem. Lett.* **2014**, 5 (12), 2058–2065.
- (77) Li, Y.; Liao, Y.; Schleyer, P. V. R.; Chen, Z. Al_2C Monolayer: The Planar Tetracoordinate Carbon Global Minimum. *Nanoscale* **2014**, *6* (18), 10784–10791.

- (78) Vogt, P.; De Padova, P.; Quaresima, C.; Avila, J.; Frantzeskakis, E.; Asensio, M. C.; Resta, A.; Ealet, B.; Le Lay, G. Silicene: Compelling Experimental Evidence for Graphenelike Two-Dimensional Silicon. *Phys. Rev. Lett.* **2012**, *108* (15), 155501.
- (79) Becke, A. D.; Edgecombe, K. E. A Simple Measure of Electron Localization in Atomic and Molecular Systems. *J. Chem. Phys.* **1990**, 92 (9), 5397–5403.
- (80) Bader, R. F. W. Atoms in Molecules. Acc. Chem. Res. 1985, 18 (1), 9-15.
- (81) Tang, H.; Ismail-Beigi, S. Novel Precursors for Boron Nanotubes: The Competition of Two-Center and Three-Center Bonding in Boron Sheets. *Phys. Rev. Lett.* **2007**, 99 (11), 115501.
- (82) Galeev, T. R.; Dunnington, B. D.; Schmidt, J. R.; Boldyrev, A. I. Solid State Adaptive Natural Density Partitioning: A Tool for Deciphering Multi-Center Bonding in Periodic Systems. *Phys. Chem. Chem. Phys.* **2013**, *15* (14), 5022.

□ Recommended by ACS

Electron Counting and High-Pressure Phase Transformations in Metal Hexaborides

Harry W. T. Morgan and Anastassia N. Alexandrova

NOVEMBER 09, 2022 INORGANIC CHEMISTRY

READ 🗹

The Exotically Stoichiometric Compounds and Superconductivity of Lithium-Copper Systems under High Pressure

Mingqi Jiang, Hanyu Liu, et al.

SEPTEMBER 29, 2022

THE JOURNAL OF PHYSICAL CHEMISTRY LETTERS

READ 🗹

Cubic Stuffed-Diamond Semiconductors $LiCu_3TiQ_4$ (Q=S, Se, and Te)

Michael A. Quintero, Mercouri G. Kanatzidis, et al.

JULY 07, 2022

JOURNAL OF THE AMERICAN CHEMICAL SOCIETY

READ 🗹

Path Less Traveled: A Contemporary Twist on Synthesis and Traditional Structure Solution of Metastable LiNi₁₂B₈

Gourab Bhaskar, Julia V. Zaikina, et al.

JUNE 10, 2022

ACS MATERIALS AU

READ 🗹

Get More Suggestions >